:NTATION PAGE

Form Approved
OMB No. 0704-0188

nated to average 1 hour per response, including the time for reviewing instructions, searching existing data sources, reviewing the collection of information. Send comments regarding this burden estimate or any other aspect of this burden, to Washington Headquarters Services, Directorate for Information Operations and Reports, 1215 Jefferson Office of Management and Budget, Paperwork Reduction Project (0704-0188), Washington, DC 20503.

2. REPORT DATE	3. REPORT TYPE AND DATES COVERED
17 June 1994	Final 01 Oct 93- 01 Apr 94

4. TITLE AND SUBTITLE

Numerical Studies of Low Temperature Gallium Arsenide Buffer Layers and their Influence on Device Operation

5. FUNDING NUMBERS

~~F49620-91-C-0016~~
61102F
2305/BS

6. AUTHOR(S)

Harold L. Grubin and John P. Kreskovsky

7. PERFORMING ORGANIZATION NAME(S) AND ADDRESS(ES)

Scientific Research Associates, Inc.
50 Nye Rd., P.O. Box 1058
Glastonbury, CT 06033

8. PERFORMING ORGANIZATION REPORT NUMBER

AFOSR-TR- 94 0402
R94-9134-F

9. SPONSORING/MONITORING AGENCY NAME(S) AND ADDRESS(ES)

Dr. Gerald Witt, AFOSR/NE
Directorate of Electronic and Material Sciences
110 Duncan Ave., Suite B115
Bolling AFB, DC 20332-0001

10. SPONSORING/MONITORING AGENCY REPORT NUMBER

F49620-91-C-0016

11. SUPPLEMENTARY NOTES

36pp

12a. DISTRIBUTION/AVAILABILITY STATEMENT

Approved for public release;
distribution unlimited.

13. ABSTRACT *(Maximum 200 words)*

Through the use of numerical methods involving both the drift and diffusion equations including traps, and more recently the quantum Liouville equation, Scientific Research Associates, Inc., (SRA) has been examining the physics and operation of LTG materials and devices. Both defect and Schottky models have been studied, and two-dimensional microscopic and macroscopic device simulations have been performed. A new generalization of the drift and diffusion equations, including current, has been implemented for the specific purpose of treating embedded metallic precipitates. This document summarizes SRA work under U.S. Air Force, Office of Scientific Research, Contract # F49620-91-C-0023.

14. SUBJECT TERMS		15. NUMBER OF PAGES
Gallium Arsenide	Low Temperature	35
Precipitates	Defects	16. PRICE CODE
Traps	Buried Schottky Barriers	

17. SECURITY CLASSIFICATION OF REPORT	18. SECURITY CLASSIFICATION OF THIS PAGE	19. SECURITY CLASSIFICATION OF ABSTRACT	20. LIMITATION OF ABSTRACT
Unclassified	Unclassified	Unclassified	UL

Scientific Research Associates, inc.

50 Nye Road, P.O. Box 1058
Tel: (203) 659-0333

Glastonbury, Connecticut 06033
Fax: (203) 633-0676

Final Report

NUMERICAL STUDIES OF LOW TEMPERATURE GALLIUM ARSENIDE BUFFER LAYERS AND THEIR INFLUENCE ON DEVICE OPERATION

Harold L. Grubin and John P. Kreskovsky

SRA R94-9134-F

Contract F49620-91-C-0023

Submitted to
Air Force Office of Scientific Research
110 Duncan Avenue, Suite B115
Bolling AFB, DC 20332-0001

June 1994

Approved for Public Release;
Distribution Unlimited

Approved for public release;
distribution unlimited.

NUMERICAL STUDIES OF THE PHYSICS AND OPERATION OF LTG MATERIALS AND DEVICES

TABLE OF CONTENTS

NUMERICAL STUDIES OF THE PHYSICS AND OPERATION OF LTG MATERIALS AND DEVICES

ABSTRACT

Through the use of numerical methods involving both the drift and diffusion equations including traps, and more recently the quantum Liouville equation, Scientific Research Associates, Inc., (SRA) has been examining the physics and operation of LTG materials and devices. Both defect and Schottky models have been studied, and two-dimensional microscopic and macroscopic device simulations have been performed. A new generalization of the drift and diffusion equations, including current, has been implemented for the specific purpose of treating embedded metallic precipitates. This document summarizes SRA work under U.S. Air Force, Office of Scientific Research, Contract # F49620-91-C-0023.

NUMERICAL STUDIES OF THE PHYSICS AND OPERATION OF LTG MATERIALS AND DEVICES

1. INTRODUCTION

Molecular beam epitaxy (MBE) GaAS is normally grown at substrate temperatures near 600C, as this produces (i) materials with shallow donor and acceptor concentrations in the range of $10^{13}/cm^3$ and (ii) deep traps at least an order of magnitude smaller. Growth at lower temperatures, (e.g., 500C) has led to higher concentrations of traps[1], and in some early studies, to semi-insulating materials with resistivities in the range of[2] $3x10^4$ ohm-cm. The present high interest in low temperature growth material stems from the pioneering studies of Smith et al.[3], who showed that by employing a buffer grown at 200 C and annealed to 600 C, backgating and light sensitivity could be eliminated.

GaAs grown by MBE at 200 to 250 C is not semi-insulating without an anneal above 500C. Growth at these temperatures produces a high concentration of the anion antisite defect, As_{Ga}, which is the dominant point defect in As-rich GaAs. The anion antisite defect, As_{Ga}, was determined, more than 10 years ago, to be a double donor with a mid gap level; it is commonly called EL2. This defect has been identified in as-grown LT layers in concentrations up to $10^{20}/cm^3$, which is high enough to result in hopping conduction between localized defects, rendering LT GaAs conductive.

After annealing, the concentration of defects in LT GaAs drops by at least two orders of magnitude, and is accompanied by the formation of As precipitates[4]. The nature of the precipitates has become a controversial issue with the question arising as to whether the As precipitates form buried Schottky barriers[5], and thus

---

[1] R. A. Stall, C.E.C. Wood, P. D. Kirchner and L. F. Eastman, *Electron. Lett.*, **16**, 171 (1980).

[2] T. Murotani, T. Shimanoe and S. Mitsui, *J. Cryst. Growth*, **45**, 302 (1978).

[3] F. W. Smith, A. R.Calawa, C..L. Chen, M. J. Manfra and L. J.Mahoney, *IEEE Electron Deviec Lett.*, **9**, 77 (1988)

[4] M. R. Melloch, N. Otsuka, J. M. Woodall, A. C,. Warren and J. L. Freeouf, *Appli. Phys. Lett.* **57**, 1531 (1990), and Z. Lilienthal-Weber, A. Claverie, J. Washburn, F. Smith and A/. R. Calawa, *Appl. Phys.* **A54**, 141 (1991).

[5] A. C. Warren, J.M. Woodall, J. L. Freeouf, D. Grischowsky, D. T. McInturnff, M. R. Melloch and S N. Otsuka, *Appl. Phys. Letts*, **57**, 1331 (1990).

deplete the material of carriers, or whether the residual As_{Ga} antisite defects dominate the electronic properties of annealed LT GaAs[6].

Under AFOSR Contract # F49620-91-C-0023, Scientific Research Associates, Inc. (SRA) has performed numerical studies of LT grown material with emphasis on three areas:

1. the understanding of the *microscopic* physics of discrete clusters in low temperature (LT) GaAs, with both the Schottky and defect models being considered;
2. how clusters affect current flow; and
3. the development of *macroscopic* models of LT GaAs for use in device simulation.

This document summarizes these studies.

2. SRA's STUDIES

2.1 Microscopic Studies

Under the topic of microscopic physics, SRA's efforts dealt with the following two models for studying the electrical characteristics of the annealed LTG material:

1. The material is composed of a concentration of point defects represented by deep levels of donor and acceptor traps;
2. The material is composed of a concentration of Schottky barrier-like precipitates.

We have found, with respect to the charge and current distributions, *that both the trap model and the Schottky barrier model yield similar results*, in that discrete clusters modeled using either approach render the surrounding material semi-insulating, due to overlapping depletion regions. The means to resolve which of these models, or perhaps what combination of the two is correct, is discussed.

2.2 Macroscopic Studies

While it is necessary to develop a discrete model of LT GaAs clusters to gain insight and understanding of the flow of electrons around and through the maze such clusters create in LT layers, it is also necessary to translate these results and understanding thus gained into a macroscopic model of LT GaAs material.

---

[6] D. C. Look, *Thin Solid Films*, **231**, 61 (1993).

This need arises when one considers the potential uses of LT GaAs in device fabrication.

LT GaAs is presently being considered for use in gate isolation layers and buffer layers to reduce back and side gating effects in FETs. With such contemplated uses it realized that the dimensions of such layers may be orders of magnitudes above the 10 Å to 100 Å length scales associated with discrete clusters. As a result, the microscopic details of the current paths through the LT material are of reduced interest. What is important, from the standpoint of device operation, is the degree of isolation the LT layer provides, the capacitive effects of the layer, how this affects transient response, and how the breakdown characteristics are altered by a gate isolation layer. Such parameters are likely to be adequately predicted by an averaged macroscopic model. Such a model is necessary for present and near future full device simulations, otherwise millions of grid points could be required for 2D FET studies. For example, an FET structure considered under the present effort had a source-drain spacing of 3.5 μm, a 0.1 μm deep channel and a 0.2 μm deep LT buffer layer. If we assume that discrete clusters are randomly distributed in the LT region, and a grid spacing of 10 Å is required to give reasonable resolution of the clusters, then *700,000 grid points* would be required to resolve the buffer layer alone! While from a purely physics viewpoint, discrete cluster modeling is preferable; it is impractical from a device simulation viewpoint. The details of our approach to macroscopic modeling of LT materials will also be discussed.

3. THE TRAP MODEL OF DISCRETE CLUSTERS

Recently, considerable research has been performed in an effort to understand observed favorable properties of GaAs grown by molecular beam epitaxy (MBE) at low temperatures of about 200°C. Depending on the precise growth temperature and subsequent annealing, low temperature (LT) GaAs buffer layers have been found to reduce backgating, sidegating and light sensitivity in GaAs MESFETs. These LT buffer layers are typically highly resistive, even when Si doped to levels greater than $10^{18}/cm^3$. Such characteristics are attributed to the presence of As precipitates which, it has been suggested, act as buried Schottky barriers (reference 5), depleting the region around them of mobile carriers. Providing the spacing between the As precipitates is small enough, the depletion regions will overlap and render the LT GaAs material highly resistive. It has also been

suggested[7] that the precipitates exhibit properties similar to those of the EL2 defect. It has further been suggested that deep acceptors, 0.3 ev above the valence band, are present in P-type LT GaAs[8].

In the trap model of the LT GaAs the cluster is represented by donor and acceptor traps; and while only single levels of donor an acceptor traps are discussed below, present efforts are underway to incorporate multiple levels. We also assume transport is governed by the continuity equations for electrons and holes, including generation and recombination:

$$(1) \qquad \frac{\partial n}{\partial t} = \frac{1}{e}\nabla \cdot J_n + G_n - R_n$$

$$(2) \qquad \frac{\partial p}{\partial t} = -\frac{1}{e}\nabla \cdot J_p + G_p - R_p$$

These equations identify local time dependent changes in electron n, and hole, p, carrier density. J_n and J_p represent the current density of electrons and holes. G and R represent the net generation and recombination that include capture and emission of electrons and holes by deep level trapping centers.

The kinetics of capture and emission from donors and acceptors determine the recombination rates for electrons, R_n, and holes, R_p, introduced into equations (1) and (2).

$$(3) \qquad G_n - R_n = C_n\left(n_1^a N_A^- - nN_A^0\right) + C_n^+\left(n_1^d N_D^0 - nN_D^+\right)$$

where C_n^+ and C_n denote capture rates of electrons from acceptors and donors, respectively. For holes the net recombination rate is:

$$(4) \qquad G_p - R_p = C_p^-\left(p_1^a N_A^o - pN_A^-\right) + C_p\left(p_1^d N_D^+ - pN_D^o\right)$$

---

[7] M. O. Manaresh, D. C. Look, K. R. Evans and C. E. Stitz, *Phys. Rev.* **B41**, 10271 (1990)

[8] M. Kaminska, E. R. Weber, Z. Liliental-Weber, R. Leon and Z. U. Rek, *J. Vac. Sci. Tech.*, **B&**, 710 (1989).

where C_p^- and C_p denote capture rates of holes from acceptors and donors, respectively. The n_1 and p_1 terms are obtained from equilibrium conditions, and under nondegenerate conditions are approximated by the equations:

$$(5) \qquad n_1^a = N_c \exp-\left((E_c - E_a)/k_B T\right), \quad n_1^d = N_c \exp-\left((E_c - E_d)/k_B T\right)$$

$$(6) \qquad p_1^a = N_v \exp-\left((E_a - E_v)/k_B T\right), \quad p_1^d = N_v \exp-\left((E_d - E_v)/k_B T\right)$$

The filling and emptying of the donor and acceptor states occurs during a finite time period and is governed by the same kinetics as discussed above. For a single acceptor level and a single donor level the rate of change of the population of these levels is given by

$$(7) \qquad \frac{\partial N_A^-}{\partial t} = C_p^-\left(p_1^a N_A^o - p N_A^-\right) + C_n\left(n N_A^o - n_1^a N_A^-\right)$$

$$(8) \qquad \frac{\partial N_D^+}{\partial t} = C_n^+\left(n_1^d N_D^o - n N_D^+\right) + C_p\left(p N_D^o - p_1^d N_D^+\right)$$

The above equations (1), (2), (7), and (8) identify several components of the continuity equation. The constitutive relationships for current density are given below:

$$(9) \qquad J_n = -e\left(n\mu_n \nabla\psi + \phi_n - D_n \nabla_n\right)$$

$$(10) \qquad J_p = -e\left(p\mu_p \nabla\psi + \phi_p - D_p \nabla_p\right)$$

where ϕ_n and ϕ_p account for variations in the band structure arising from material interfaces.

Finally, Poisson's equation is introduced as

$$(11) \qquad \nabla \bullet \varepsilon \nabla\psi = e\left(n - p - \langle c \rangle\right)$$

where $\langle c \rangle$ is the net concentration of ionized donors and acceptors arising from both deep level traps, as well as shallow dopants. In the present model, the deep

level traps represent the As clusters, whereas the shallow, fully-ionized dopants represent the doping level of the surrounding GaAs material.

3.1 Defect Model Simulations-One Dimension and Single Cluster

Four groups of simulations were performed. The first simulation series was a one-dimensional study of a single cluster placed symmetrically at the center of a one-micron structure. The cluster was 100Å in diameter. The various simulations delineate the effect of varying the nominal doping surrounding the cluster. For this study both *N* and *P* type material were considered. The ratio of deep level donors to acceptors was varied. For $N_D/N_A = 1.014$, $E_C - E_F = 0.8$ ev in the cluster. Provided the density of deep level donors and acceptors is high enough, the surrounding material will be depleted of mobile carriers (through trapping within the cluster). In the present simulations the nominal trap level was $10^{20}/cm^3$. Additional simulations were performed for different values of the nominal trap level. All results showed similar qualitative behavior, although the quantitative behavior differs. In particular, the mobile electrons (holes) surrounding the cluster would diffuse into the cluster and neutralize deep level donors (acceptors). The region surrounding the cluster is depleted of mobile charge and a potential distribution similar to that at a Schottky barrier is established. The height of the potential barrier is dependent on the density of the shallow dopants surrounding the cluster, since the trap kinetics within the cluster determine the electron density within the cluster, which in turn depdends upon the surrounding doping level.

An example of such a result is given in figure 1, where the electron concentration, potential and space charge are displayed for the case of $E_C - E_F = 0.8$ and shallow donors at $1x10^{17}/cm^3$. For this calculation we have taken advantage of the symmetry and are plotting only the right-hand portion of the calculation. Further, the abscissa is the square root of distance. This allows us to exaggerate the position dependence of density and potential within the center of the structure.

As seen in figure 1, the density within the cluster shows a value somewhat below $10^5/cm^3$, increasing to the shallow donor level of $10^{17}/cm^3$ away from the cluster. This variation in density is responsible for the built-in potential, which is the difference in value of the potential at the beginning and center of the structure. The extent of the region of charge depletion is shown in the third frame, which represents the net carrier density: [*n-p-net ionized charge (including traps)*]. Thus we see that approximately 600 Å of the structure is depleted of charge.

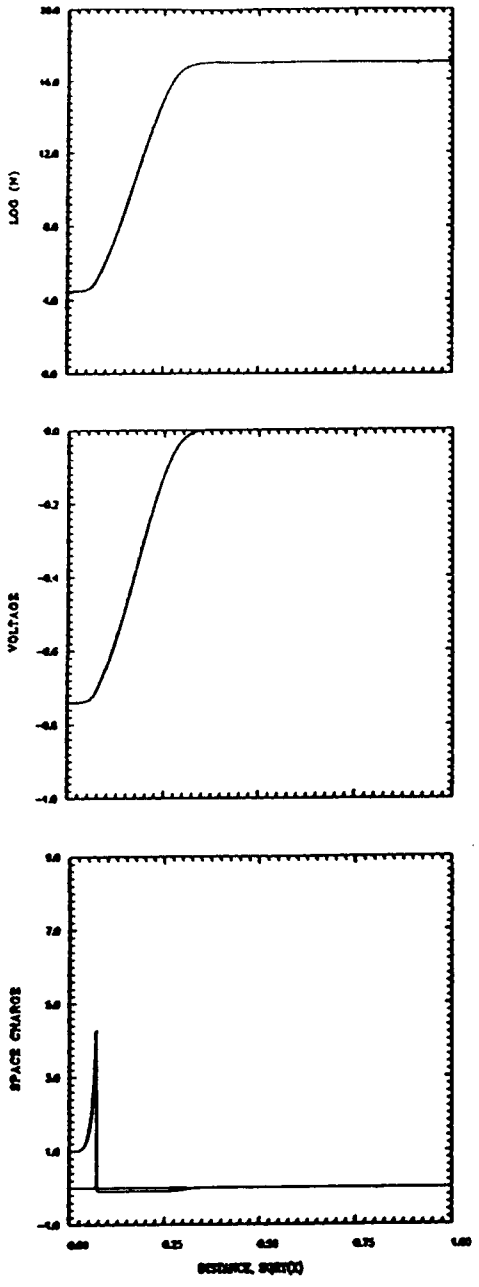

Figure 1. Density, potential, and net charge density for a 100 Å cluster embedded in a two micron structure.

3.2 Defect Model Simulations-One Dimension and Two Clusters

The second series of simulations performed was for a structure representing two clusters separated by 300 Å. These simulations were also performed for a range of shallow dopant densities. For doping levels below $10^{18}/cm^3$ (*N* or *P* type), the region between the clusters was completely depleted and the material is semi-insulating. As the doping level exceeded $10^{18}/cm^3$, the clusters were unable to fully deplete the surrounding material and the insulating properties are reduced. This result is consistent with the conclusions of Ref. 5 (even though the description here is not that of a Schottky barrier, but of depletion due to defects). It should be recognized, however, that the exact limits of where significant conduction would begin to occur would depend on the trap kinetics and deep level densities specified in the model. An example of the potential, electron and space charge distribution between the two clusters is shown in figure 2, again for $E_C - E_F$ = 0.8 and shallow donors of $4x10^{18}/cm^3$. The material is just beginning to exhibit conductive properties.

The first frame of figure 2 displays the density, which shows an increase toward the center of the structure. There is still charge depletion at the center. The concentration of carriers within the cluster region is again somewhat below $10^5/cm^3$. As seen in the third frame, the density between the clusters is negligible.

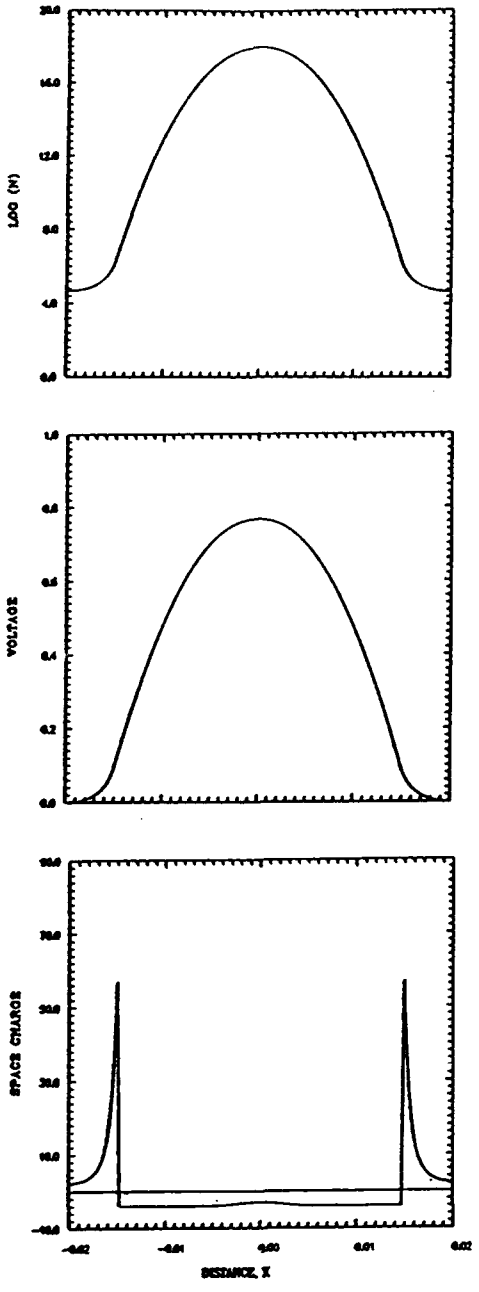

Figure 2. Density, potential, and net charge density for dual 100 Å clusters separated by 300 Å. (Distance is in microns.)

3.3 Defect Model Simulations-Two Dimensions

The third group of simulation studies of discrete clusters involves two-dimensional arrays of clusters. Here, clusters 75 Å in diameter are separated by 125 Å. Two rows of clusters were considered, along with two different groupings. In one case the clusters in the two rows are aligned such that four clusters, two from each row, formed the corners of a square. In the second case the clusters are staggered such that three clusters create a triangle. The second group of simulations are illustrated in figure 3. Such simulations are useful in studying material properties and device characteristics which would be required in a macroscopic model. Particular emphasis is placed on the current paths, if any, and the possibility of breakdown. Typical results for a staggered cluster arrangement are shown in figure 3 at a bias of 0.5 volts. Here the bulk material is $10^{18}/cm^3$ *N* type. The effect of the overlapping depletion region is apparent, in that mobile charge is heavily depleted between the clusters. However, with the application of bias, some charge is being injected into the structure. The potential distribution in the region of charge injection shows lower values of field, while at the anode side there is considerable charge depletion and a concomitant large potential drop. The field at the anode is very high, the current is negligible, and we have provisionally concluded that a structure of this type would show low currents, followed by catastrophic breakdown.

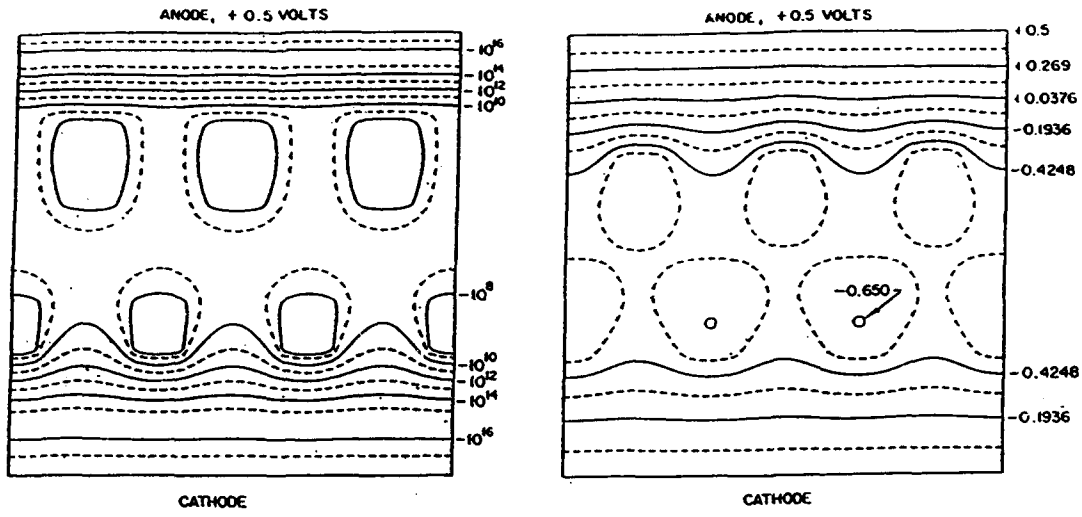

Figure 3. Two-dimensional simulation of the density and potential profiles of staggered arrays of clusters with a diameter of 75 Å, separated by 125 Å , embedded in a square 600 Å on edge. Left figure shows contours of constant density under an applied voltage of 0.5 volts. Right figure shows contours of constant potential.

An earlier set of calculations was performed for a set of clusters randomly placed in a two-dimensional *NIN* configuration. This calculation, which is displayed in figure 4, was performed for an array of clusters that were larger than those commonly observed, but does display the types of streamlines to be expected for carriers being transported through such an array. What should be noticed here are the percolating paths, and the resulting extremely low value of current.

Figure 4. Current streamlines in an NIN structure for V=5v. Note current paths around acceptor clusters The mean current is less than 160 amp/cm^2.

4. THE SCHOTTKY MODEL OF DISCRETE CLUSTERS

Recent efforts under the present contract have been directed towards the modeling of the discrete clusters in LT GaAs as embedded Schottky barriers. To accomplish this, it was necessary to address the issue of *how to model a metal within the framework of the drift and diffusion equations.* The steps we have taken must be regarded as initial efforts, in that Fermi statistics are ignored, as are the quantum contributions-both of which will be addressed later.

We retain the drift and diffusion equations in the analysis of the Schottky model, and for the metal we ignore the band gap in the equations. We further assume that $N_i = N_C = N_V$, and choose effective masses for electrons and holes to yield values of N_c and N_V, which are consistent with the electron density in a metal. (For our initial calculations we chose an effective mass to yield $N_C = N_V = 10^{20}/cm^3$. While this value is somewhat low for metals, it yields a free electron concentration substantially higher than that in the adjacent semiconductor and provides *metal-like* behavior). The holes are taken to play the same role as the ionized background in metals, and we set the hole mobility to zero within the framework of the drift and diffusion equations. We have set the electron mobility to 10,000 cm^2/volt-sec in our initial simulations.

From the band diagram of a Schottky barrier, it is recalled that the barrier heights is given by $\phi_{Bn} = q(\phi_m - \chi_s)$ for electrons, where ϕ_m is the work function of the metal and χ_s is the electron affinity of the semiconductor. The interface between our modeled metal and the semiconductor are to be treated using a heterojunction formulation. Here, effective potentials are introduced in the drift terms to account for the variation in the band structure across an interface, as noted in Eqs. (9) and (10). These effective potentials are given by

$$(12) \quad \phi_n = \frac{kT}{q} \ell n N_C + \chi_s$$

for electrons and

$$(13) \quad \phi_p = -\frac{kT}{q} \ell n N_V + \chi_s + E_g$$

for holes. For the 'metal' we set the effective 'metal electron affinity" equal to the workfunction. Thus, given the barrier height and the semiconductor electron af-

finity, the metal workfunction and our effective 'metal electron affinity" are determined, as are ϕ_n and ϕ_p.

In performing the Schottky calculations, we have also included the effects of traps at the interface, as these are usually present at metal/GaAs interfaces, and have included calculations of current. While these contributions may not seem extraordinary, it is emphasized that *these calculations include the effects of the metal as part of the governing equations, rather than as boundary condition*. This represents a major advance in the modeling aspects of the problem.

4.1 Schottky Model Simulations-One Dimension, Single Cluster, No Traps

We have performed a variety of simulations of Schottky barriers using this model for both N and P type material. The structure consists of a 200 Å metallic precipitate embedded within a 4000 Å thick section of GaAs. The semiconductor material was doped to $10^{17}/cm^3$ (N or P type).

Figure 5 shows the electron density and band structure for a Schottky barrier precipitate of 0.8 ev on N type material at zero bias. Again we are showing only one half of the calculation. The results are those of a classical Schottky barrier. The flat line at the left of the energy band profile represents the top of the valence band of the 'metal'. Note that the density at the interface between the metallic precipitate and the semiconductor is approximately the same as the density shown in figure 1. Indeed, the depletion layer thickness is approximately the same as figure 1, with the differences attributed to the slight differences in the barrier height. Note that we have arbitrarily chosen the energy level in the metal as zero. Figure 6 shows similar results for a 0.4 volts forward bias. Here we observe a reduction in the width of the depletion layer and an increase in the electron density at the interface. Again the results are consistent with results of the trap defect model. The electron density increases in proportion to $e^{q\Delta V/kT}$, where ΔV is the change in the local potential.

4.2 Schottky Model Simulations-One Dimension, Single Cluster, Traps

The next results show the effect of introducing a 10 Å layer of traps at the interface. When the ratio of donors and acceptor traps is such that $(E_c - E_f)$, *in the trap region* is 0.8 ev (which is also the barrier height), the traps have little effect on the distribution of charge and potential at zero bias. When the trap concentrations are adjusted to give a value of 0.6 ev for $(E_c - E_f)$ under equilibrium conditions, the results are as shown in figure 7. Here we see an increase in electron density across

the trap region and a corresponding alteration in the conduction and valence band structure. The barrier height remains at 0.8 ev, but to the right of the trap layer the apparent barrier height is reduced. The narrow spiked barrier across the trap layer is probably thin enough to be penetrated by tunneling at low bias levels; however, this would require quantum corrections to be added to the model to accurately predict this effect. When the level of traps is adjusted so that $(E_c - E_f) = 1.0$ ev in the trap layer, the results appear as in figure 8. The barrier height is increased.

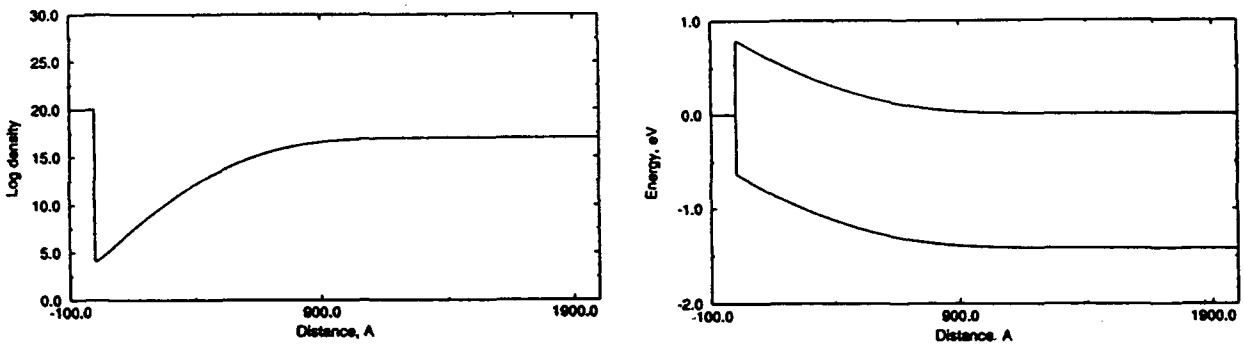

Figure. 5 Density, conduction and valence band energies for a metallic precipitate 'Schottky' barrier with a barrier height of 0.8ev. No traps in this calculation.

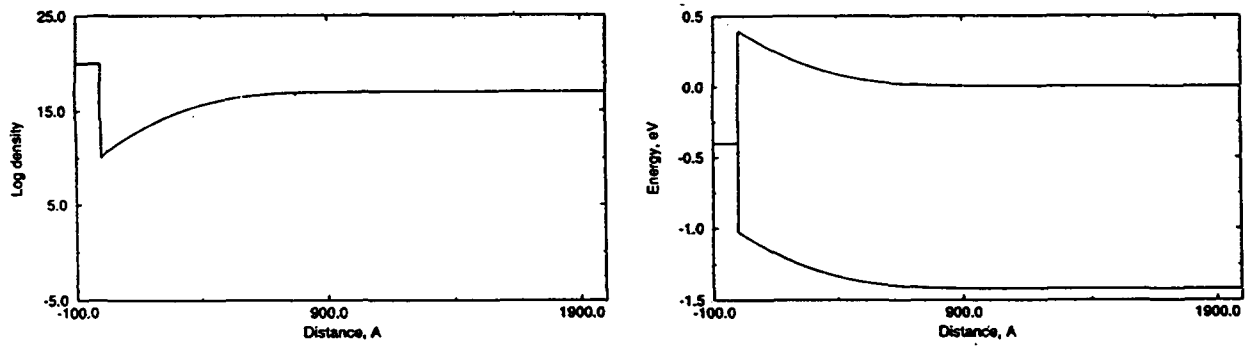

Figure 6. Density, conduction and valence band energies for a metallic precipitate 'Schottky' barrier with a barrier height of 0.8ev. No traps in this calculation. Calculation is under forward bias of 0.4 volts.

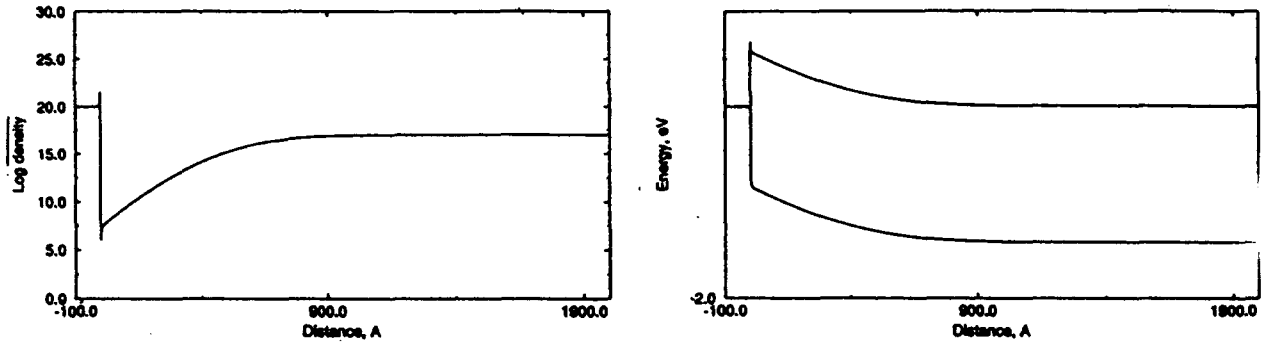

Figure 7. Density, conduction and valence band energies for a metallic precipitate 'Schottky' barrier with a barrier height of 0.8ev. A 10 Å layer of traps with $E_F - E_C = 0.6ev$ is at the interface.

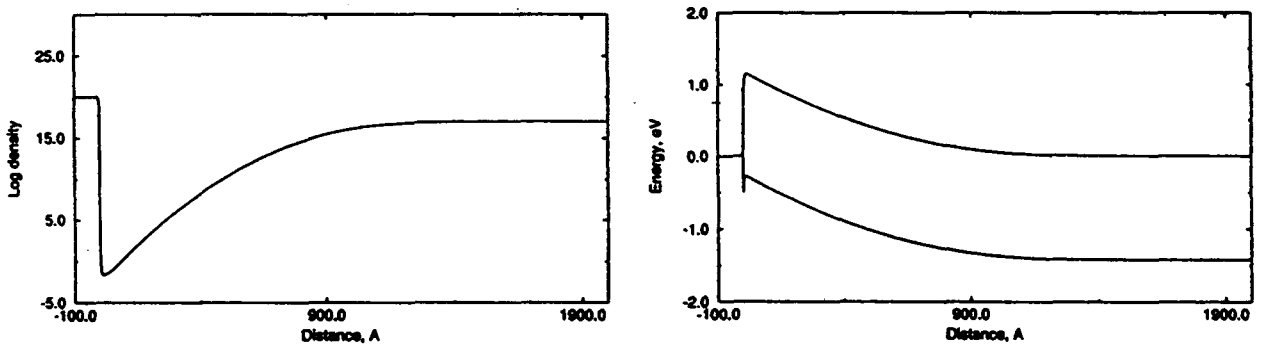

Figure 8. Density, conduction and valence band energies for a metallic precipitate 'Schottky' barrier with a barrier height of 0.8ev. A 10 Å layer of traps with $E_F - E_C = 1.0ev$ is at the interface.

A comparison of figures 7 and 8 points out that traps at the boundary of a Schottky interface will have a profound effect on the distribution of charge surrounding the precipitate. In the case of the figure 7 calculations, there is a reduction in the depletion layer thickness, as the structure displays an enhanced electron concentration in the vicinity of the barrier. For the case of figure 8, where the

equilibrium quasi-Fermi level moves further away from the conduction band, there is a decrease in the numbers of electrons in the vicinity of the Schottky barrier, and an increase in the depletion layer thickness of the N-type material.

To test the Schottky barrier model under dynamic conditions we applied a bias to a structure with one barrier to see if we could reproduce standard results with the drift and diffusion code. Future studies require that this be performed with multiple barriers. The results were gratifying, in that we were able to compute IV and account for differences in contributions due to different trap configurations at the interface.

Figure 9 shows the predicted current voltage characteristics for the case of zero traps, a trap level yielding $(E_c - E_f) = 0.8$ ev, and a trap level yielding $(E_c - E_f) = 1.2$ ev. We note that at low bias level, when traps are present and $(E_c - E_f) = 0.8$ ev, there is no difference in the current compared to the no trap case. As the bias increases, the case with zero traps shows an increase in current following an exponential relationship. When traps are present there is a delay in the final exponential growth. This delay is being investigated. When $(E_c - E_f) = 1.2$ ev there is a reduced initial current, but a similar plateau, before the exponential rise. This bias dependence of current is being investigated. Clearly a comparison of the detailed IV relation for the defect model of LTG material and the Schottky model needs to be explored.

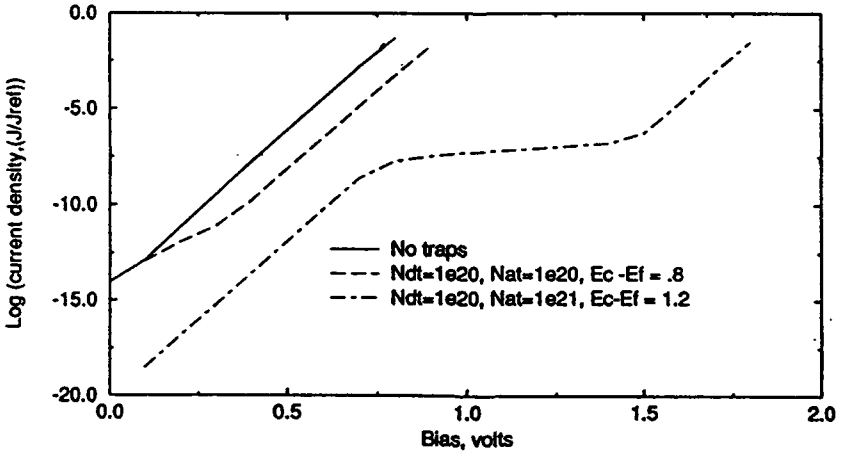

Figure 9. Current versus voltage for the Schottky precipitate model with different concentrations of traps at the interface.

We have also performed a variety of simulations for *P* type material with no alteration to the model other than the change in the doping of the semiconductor material. The results were as expected and qualitatively similar to those of the *N* type material.

5. MACROSCOPIC MODELING OF LT GaAs LAYERS

The results presented in the previous two sections show the directions pursued in modeling discrete clusters in LT GaAs. While these directions are crucial for developing an understanding of the electrical properties of LT materials, it is also necessary to develop *macroscopic* models of LT GaAs *to allow simulations* of devices of realistic sizes to be performed. Thus, there are two relevant areas of research:

1. material research where the microscopic models are appropriate, and
2. device research where the limitations of computer resources require the use of a macroscopic model for now, and in the foreseeable future.

The semi-insulating properties of LT GaAs arise largely due to the overlapping of depletion regions surrounding the clusters of excess As. The fact that traps will play an important role is a reasonable conclusion. However, on a macroscopic scale the path is somewhat different. We have shown that through the introduction of donor and acceptor traps we can establish a barrier of varying heights, which is dependent upon the ratio of donor to acceptor traps. The questions which then arise include: What are the current voltage characteristics of bulk LT GaAs? How does the material break down? How do anneal and operating temperatures affect conduction? All of these questions must be answered through experiment and analysis. This being given, how do we proceed to develop a macroscopic model?

If we refer to our trap model, then the arguments can initially focus on charge. In the trap model, the semi-insulating properties of LT GaAs arise due to the ability of the clusters, or traps surrounding them, to trap charge. When the traps are filled, the depletion layers will collapse and conduction will occur. This may occur due to two different effects. The doping of the surrounding material may be increased to the point where the traps cannot absorb all of the free electrons in the surrounding material, or electrons may be injected into the material from a conductive layer adjacent to the LT material. Now, the issue on a macroscopic scale becomes one of what is the mean concentration of traps in the LT

material. The actual distribution of the trap is of less importance, since we assume the relevant device length scales are much greater than the dimensions of individual clusters. On these length scales, the traps are distributed in an isotropic manner. Thus, from the mean value theorem the mean density of traps will be

$$(14) \quad \tilde{N}_T = \frac{\int N_T dV}{\int dV}$$

If we assume that traps are uniformly distributed in the clusters, and the clusters have a volume fraction of α, then the mean trap density is given as

$$(15) \quad \tilde{N}_T = N_{Tc} \frac{\int \alpha dV}{\int dV} = \alpha N_{Tc}$$

where N_{Tc} is the trap density in the clusters. From our discrete cluster model we found that a trap level of 10^{19} to 10^{20}/cm^3 in the clusters yielded semi-insulating properties for doping levels approaching $1x10^{18}$/cm^3. From the results of experiments it is suggested that the volume fraction of clusters is about 0.01 (1% of the volume of the LT material is occupied by As clusters). Thus, on a macroscopic scale, the mean trap density is on the order of 10^{17} to 10^{18}/cm^3.

The simulations that can be performed on a macroscopic scale permit the incorporation of a layer of traps at the interface whose width is representative of a linear or matrix array of precipitates. Thus, in a FET with a 5000 Å gate sitting on top of a semiinslating layer, the trap densities can be varied in a manner that mimics the semi-insulating properties of the clusters. Several initial device simulations have been performed on FET structures to study the effect of LT GaAs layers on device operation. A schematic of the structures is shown in figure 10.

5.1 Simulations without an LT Gate Buffer Layer

The first structure considered is shown in figure 10a. Here a 0.5 micron gate GaAs FET is considered. The channel depth is 0.1 micron with a doping of $2x10^{17}$/cm^3. The source drain spacing is 2.5 microns with 0.5 micron source and drain contacts. Thus, the overall length of the device is 3.5 microns. This structure is placed on a buffer layer 0.2 microns thick. The buffer layer is modeled using our LT GaAs macroscopic model. The predicted current-voltage characteris-

tics for this structure are shown in figure 11a. Here we observe typical FET characteristics with reasonable hard saturation. The transconductance for this device at a drain bias, V_{dc} of 1.0 volts and a gate bias of V_{gs}=0.0 volts was 95 ms/mm, and the unit gain cutoff frequency at the same bias was f_t = 22 GHz.

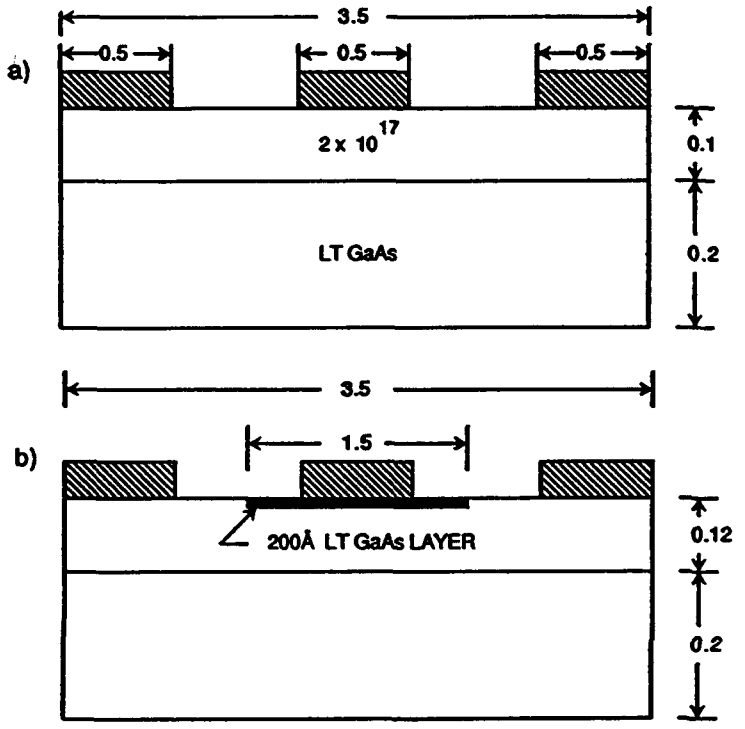

Figure 10. Schematic of structures simulated with and without a gate buffer layer.

5.2 Simulations with an LT Gate Buffer Layer

The structure was then modified, as shown in figure 10b, to include a 200 Å LT GaAs gate isolation layer. The current voltage characteristics for this device are shown in figure 11b. Here we observe that saturation is not as hard and there is less control of the device due to the displacement of the gate contact away from the GaAs channel. The channel is more conductive at any given value of gate bias. At a bias of V_{ds}=1.0 volts and V_{gs} = 0.0 volts the transconductance of this structure was close to that of the device without a gate isolation layer, at 90 ms/mm. The cutoff frequency was slightly lower at 18 GHz. This is largely due to an increase in capacitance effects associated with the gate isolation layer. As the gate bias changes, the amount of charge trapped in the LT layer varies, thus contributing to an increase in the gate capacitance.

5.3 Comparison of Simulations With and Without an LT Gate Buffer Layer

A comparison of the distribution of electrons in the two devices is shown in figure 12, where we directly observe the effect of the gate isolation layer and the LT buffer layer. (The contours are equally spaced.) Both results show little penetration of mobile charge into the buffer layer. The device with the gate isolation

layer shows additional depletion at the interface between the isolation layer and the channel, and the channel is not as highly depleted.

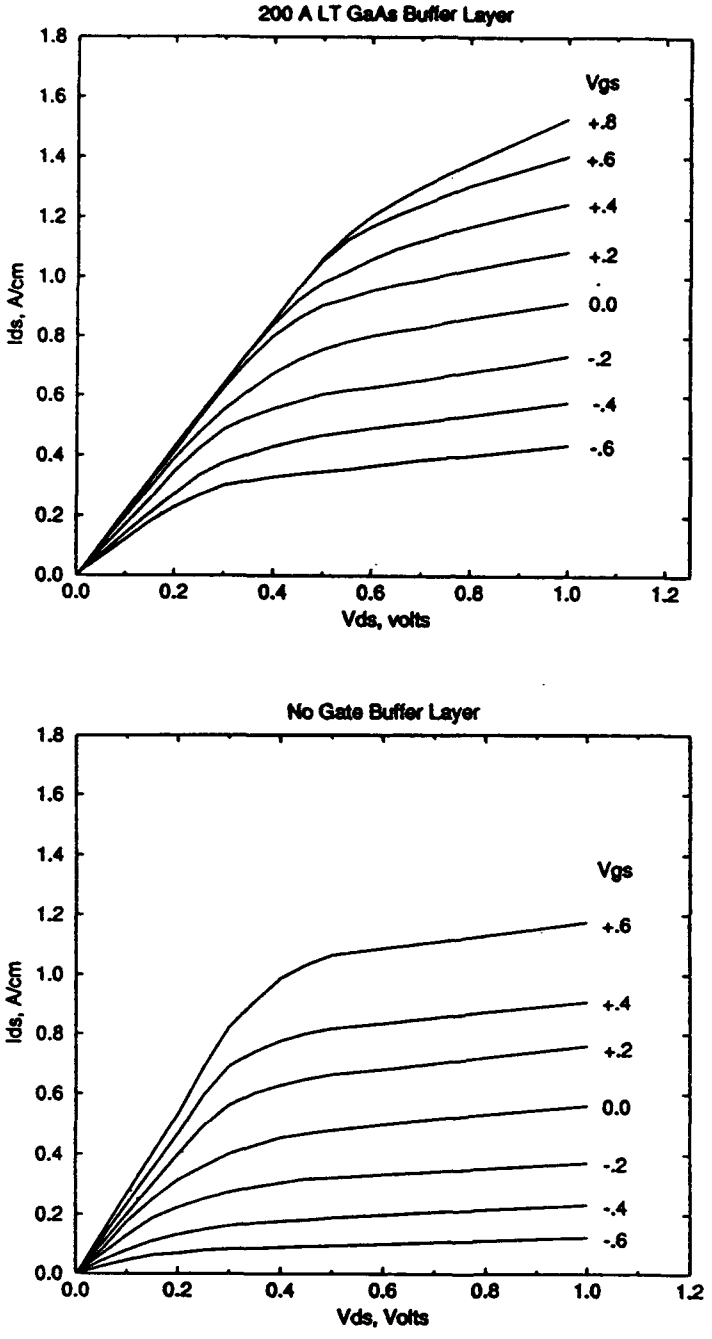

Figure 11. Current voltage characteristics for structures with and without LT gate buffer layer

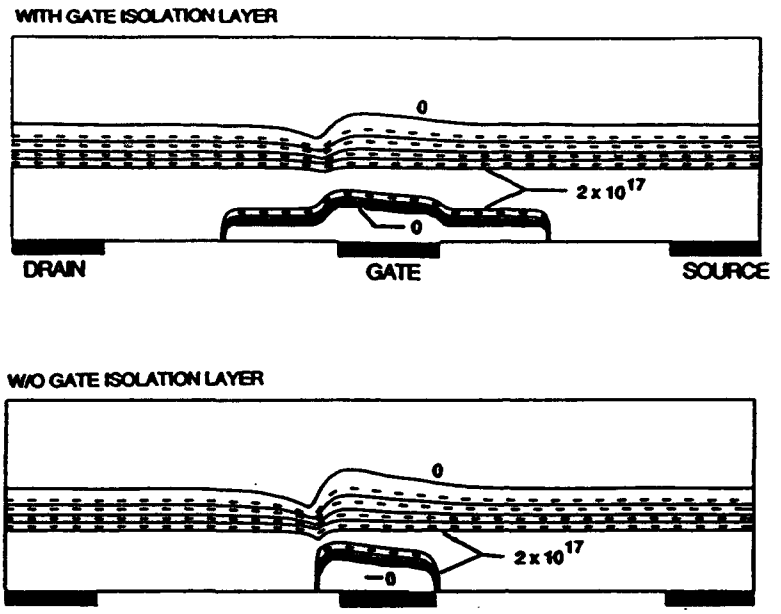

Figure 12. Contours of constant density for structures with and without an LT gate buffer. For this case V_{DS}=1.0v and V_{GS}=0.0v.

Figure 13 shows the corresponding potential distributions. The key difference here is the spreading out of the contours, particularly at the drain end of the gate. As a consequence, the field in this region is lower, and breakdown should be delayed. A final comparison, figure 14, presents the current streamlines. These show the current paths within the device. Here we observe that the current path is confined to the channel by the buffer layer. In the device with the gate isolation layer we also note that the current passes around this layer and further avoids the high field regions near the gate surface. This gives further indication that the breakdown characteristics of this structure should be superior to those of the device without the isolation layer. These comparisons are typical of the result over the entire bias range.

6. NEW DIRECTIONS FOR DISCRETE CLUSTER MODELING

Another area of importance which must be addressed is the role of quantum-mechanics in establishing the interaction of clusters. Length scales on the or-

der of angstroms are significant at the interface between the cluster and the surrounding material and quantum mechanical effects are likely to be significant.

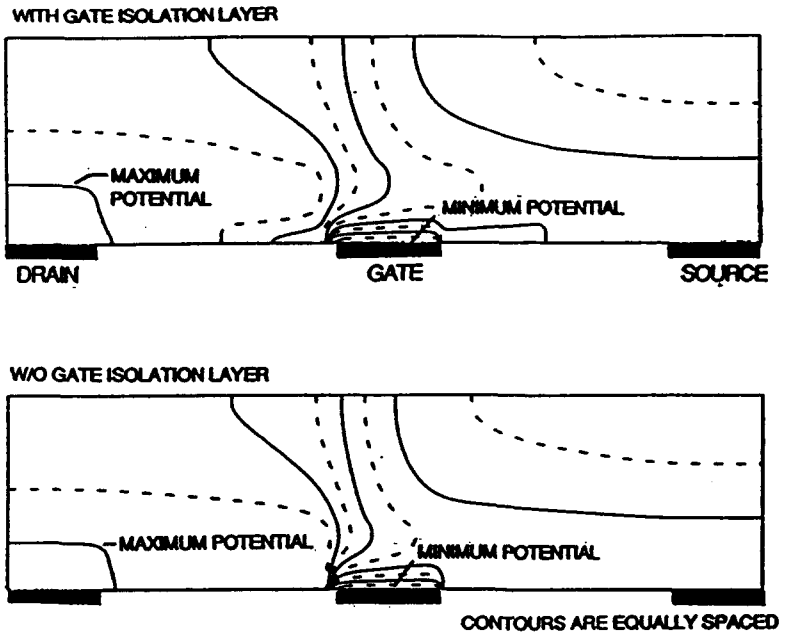

Figure 13. Contours of constant potential for structures with and without an LT gate buffer. For this case V_{DS}=1.0v and V_{GS}=0.0v.

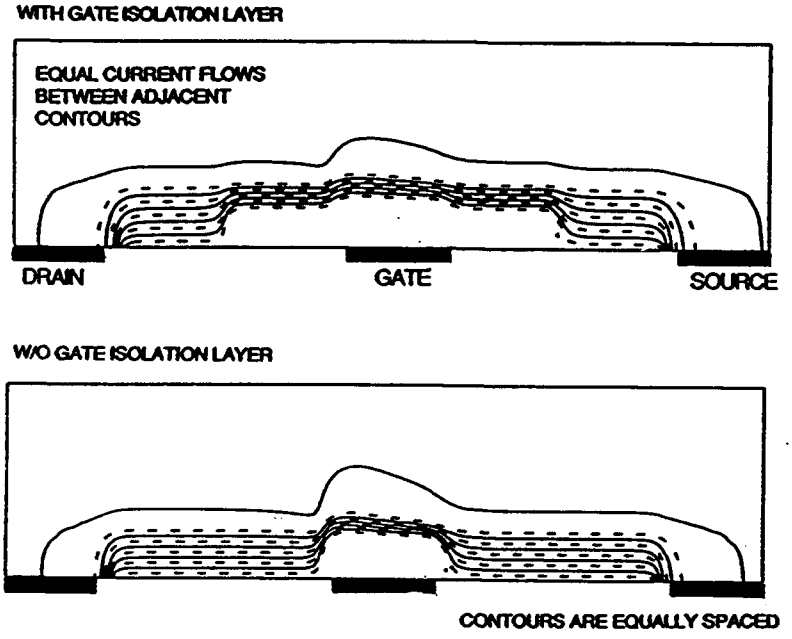

Figure 14. Current streamlines for structures with and without an LT gate buffer.

To include quantum effects within the framework of the drift and diffusion equations requires the incorporation of the quantum potential. For example, the electron continuity equation, including the quantum potential, is expressed as[9]

$$(16) \quad \frac{\partial n}{\partial t} = -\nabla \cdot n\mu\left(\psi + \phi_N + \frac{Q}{a}\right) + \nabla \cdot D\nabla n$$

Here n is the electron density, μ is the mobility, D the diffusivity, ψ the self-consistent potential, ϕ_n the potential resulting from variations in material (conduction band energy level and effective mass), and Q is the quantum potential given as

$$(17) \quad Q = -\frac{\hbar^2}{2m\sqrt{n}}\frac{\partial^2\sqrt{n}}{\partial x^2}$$

The quantity 'a' is a constant usually assigned a value of 3.0 [10]. The effect of the quantum potential is to smooth out discontinuities in the conduction band at material interfaces and allow tunneling of electrons through barrier. Extensive two dimensional simulations with the quantum potential have been underway at SRA for many years.

Less extensive, but more fundamental calculations have been performed and are treated as a check on calculations with the quantum potential. These involve the utilization of the quantum Liouville equation to examine quantum contributions.

(18)

$$i\hbar\frac{\partial <\mathbf{x}|\rho(t)|\mathbf{x}'>}{\partial t} = \left\{-\frac{\hbar^2}{2m}\left(\frac{\partial^2}{\partial \mathbf{x}^2} - \frac{\partial^2}{\partial \mathbf{x}'^2}\right) + V(\mathbf{x}) - V(\mathbf{x}')\right\} <\mathbf{x}|\rho(t)|\mathbf{x}'> + i\hbar\left\{\frac{\partial <\mathbf{x}|\rho|\mathbf{x}'>}{\partial t}\right\}_{scattering}$$

which has the form of a double Schrodinger equation. The density within the system is obtained for the case where the indices $\mathbf{x}=\mathbf{x}'$,i.e., $n(x) = <x|\rho|x>$.

---

[9] H. L. Grubin and J. P. Kreskovsky, *Solid State Electronics* 32, 1071 (1989)

[10] H. L. Grubin, T. R. Govindan, J. P. Kreskovsky and M. A. Stroscio, *Solid State Electronics*, Nov (1993).

We have implemented the Liouville equation to the study of Schottky barriers in anticipation of an application to clustering and have observed that the quantum potential is of the order of magnitude of the barrier height, indicating dominant quantum contributions at the interface[11]. Figure 15 illustrates a calculation of the effects of a delta doped region on a Schottky barrier that was formed both by a work function difference and acceptor traps. It is seen that the effects of the delta doped region are to partially collapse the Schottky barrier. These effects are of interest for the LTG problem, as the trap kinetics may dominate device performance. The calculations of figure 15 assumed a specific distribution of acceptor states; the actual trap kinetics were not introduced.

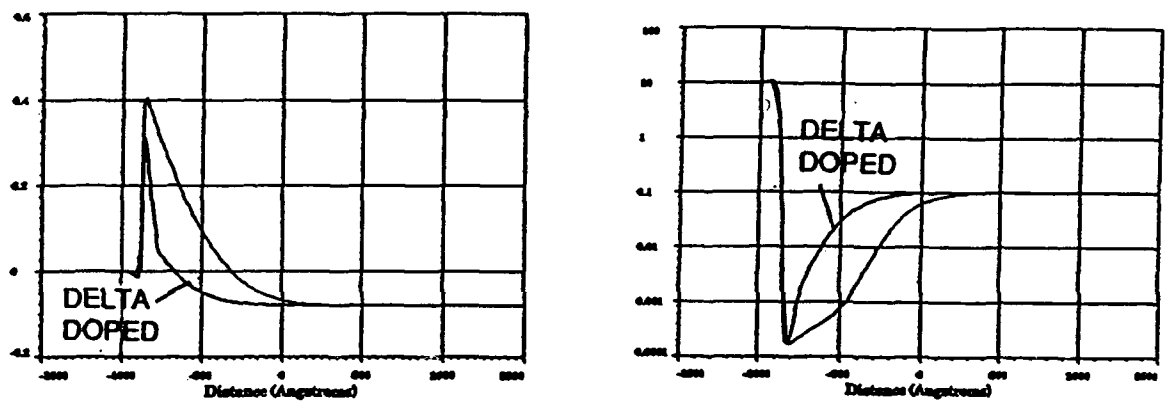

Figure 15. Density matrix calculation of a Schottky barrier and its modification due to a delta doped region. Left side is the potential energy (in ev), right side is the density in multiples of $10^{18}/cm^3$.

7. RECOMMENDATIONS

7.1 Microscopic Modeling

The electrical characteristics of the defect versus the Schottky model are likely to be marginal. Both will provide a plausible explanation for the basic high resistivity of the material. Supplemental calculations, with an emphasis on the op-

[11] H. L. Grubin, T. R. Govindan and D. K. Ferry. Presented at the *Workshop on Interfaces and Mesoscopic Systems* April 1994.

tical response of both models, as well as the temperature dependence, *should be compared to experiment.*

7.2 Macroscopic Modeling

Previously the limitations of the microscopic model, with respect to device simulation, were discussed. These limitations make it presently impossible to apply this or any microscopic model of LT GaAs to large scale device simulation. It is necessary to perform device simulations of devices using LT material if optimum design is to be achieved, and it is therefore necessary to develop models of LT GaAs on a macroscopic level. This is not a new approach. In fact, all models of semiconductor transport, except those which are based directly on first principles, are macroscopic models at some level. The moments of the Boltzmann transport equation assume a continuous sea of electrons, the result of an assumption that the mean free path between collisions is much shorter than the relevant length scales of interest. The drift and diffusion equations take matters one step further in assuming mobile carriers are in equilibrium with the local electric field. Thus, macroscopic models are common, and experience tells us they are extremely useful.

Other areas of importance are transient and high frequency response of LT GaAs. Of particular interest are two structures which have been suggested by workers at Lincoln Laboratory (figure 16). The first structure is one-dimensional in nature and consists of a Schottky barrier contact on LT GaAs. An AlAs layer is placed between the LT region and *n* type GaAs to act as a barrier. This structure sits on an N^+ GaAs substrate. Here capacitance-voltage characteristics for this structure under DC conditions, and for frequencies approaching 1 Mhz, should be determined for information connected with the trap kinetics. The second structure (figure 16b) will enable a study of gate-drain breakdown characteristics, as well as the source drain current levels.

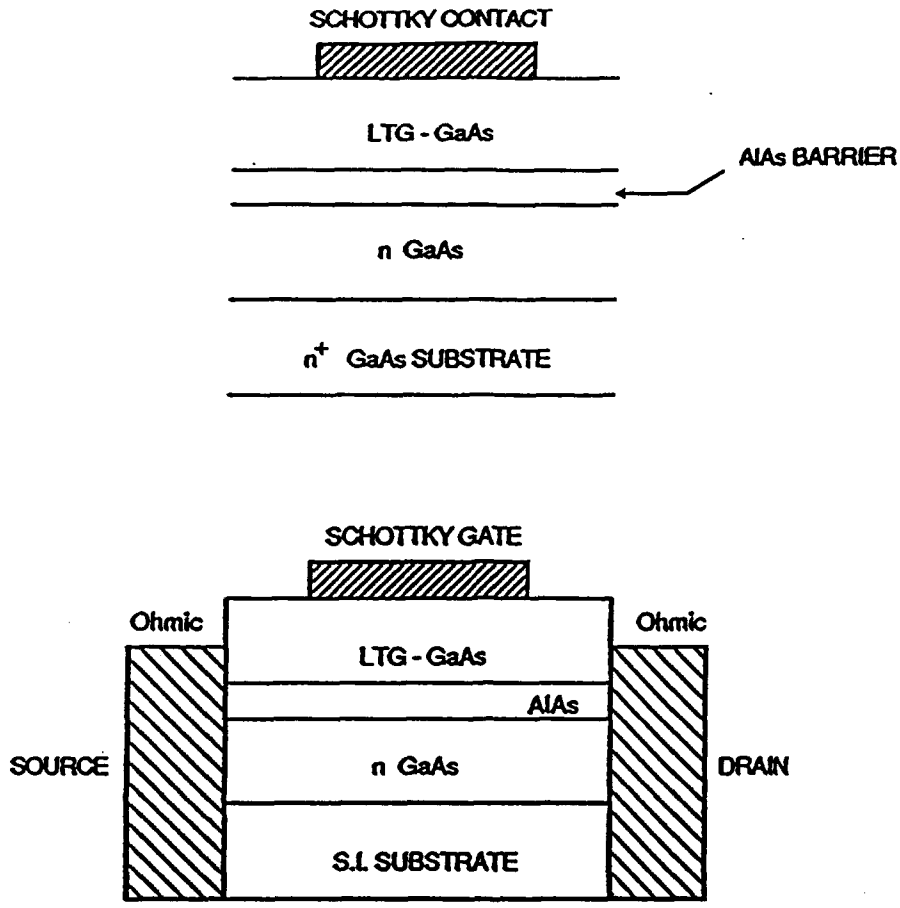

Figure 16. Schematic of structures for transient and breakdown studies.

8. REPRINTS AND LISTING OF ABSTRACTS

1. Insulating and Breakdown Characteristics of Low Temperature GaAs, *Material Research Symposium Proc.*, **241**, 39 (1992). This paper summarized the results of a model in which traps are uniformly distributed within an NIN structure, with abrupt variation in the trap density at the interface. Initial results indicated that the structure of the trap levels could provide rectifying properties. Results were consistent with later models in which the precipitates were modeled as traps.

2. Transport IN LT GaAs, *WOCSEMMAD '93*. Summarized studies of LT GaAs in which effects of precipitates are represented as traps.

3. Numerical Studies of Clusters in LT Materials, Invited paper at 1993 *APS March Meeting.*

4. Numerical Studies of the Effects of Clusters on the Electrical Characteristics of LT Gallium Arsenide. 1993 *Spring MRS Meeting*. Summarized work on clusters composed of traps, and device simulations. Work since generalized to include metallic precipitates. Paper being prepared for J. Appl. Phys.

Scientific Research Associates, inc.

50 Nye Road, P.O. Box 1058 Glastonbury, Connecticut 06033
Tel: (203) 659-0333 Fax: (203) 633-0676

Reprints

NUMERICAL STUDIES OF LOW TEMPERATURE GALLIUM ARSENIDE BUFFER LAYERS AND THEIR INFLUENCE ON DEVICE OPERATION

Harold L. Grubin and John P. Kreskovsky

SRA R94-9134-F

Contract F49620-91-C-0023

Submitted to
Air Force Office of Scientific Research
110 Duncan Avenue, Suite B115
Bolling AFB, DC 20332-0001

June 1994

INSULATING AND BREAKDOWN CHARACTERISTICS OF LOW TEMPERATURE GaAs

H. L. Grubin, J. P. Kreskovsky and R. Levy
Scientific Research Associates, Inc.
Glastonbury, Connecticut 06033

ABSTRACT

The electrical characteristics of an N(LT)N structure are studied through implementation of numerical simulation techniques for the case of donor traps 0.83 ev below the conduction band and acceptor traps 0.3 ev above the valence band. The results show characteristics sensitive to the relative densities of the traps. In particular, high acceptor trap / low donor trap concentrations generally result in low breakdown voltages, whereas high acceptor / high donor concentrations result in higher breakdown voltages.

INTRODUCTION

The purpose of this discussion is to briefly summarize recent calculations of the electrical characteristics of low temperature growth GaAs (LT GaAs). The device studied was a three micron N(LT)N structure with N regions characterized by shallow donors at $10^{17}/cm^3$; and an LT region characterized by a single level of acceptor traps of density P_a, located 0.3 ev above the valence band [1], and a single level of donor traps of density N_d located at 0.83 ev below the conduction band.

The results are placed in two categories: Highly resistive LT regions ($> 10^6$ ohm-cm) with (a) *low* current levels and sudden breakdown, and (b) higher current levels with gradual breakdown. Breakdown characteristics depend upon the magnitude and distribution of the field. For high acceptor / low donor trap concentrations the fields is near zero in the LT region and approaches breakdown values at the anode (LT)N interface; for other combinations the field profile is complex. The study suggests that breakdown voltages will depend upon growth and processing temperatures of LT GaAs.

THE GOVERNING EQUATIONS

The equations include rate equations for electrons and holes, acceptor and donor traps:

(1) $\partial n/\partial t - div(j_n/e) = G + \{c_{nd}[n_d N_d^0 - n N_d^+] + c_{na}[n_a P_a^- - n P_a^0]\}$

(2) $\partial p/\partial t + div(j_p/e) = G + \{c_{pa}[p_a P_a^0 - p P_a^-] + c_{pd}[p_d N_d^+ - p N_d^0]\}$

(3) $\partial P_a^- /\partial t = -e_2 P_a^- + e_3 P_a^0$

(4) $\partial N_d^+ /\partial t = -e_4 N_d^+ + e_1 N_d^0$

Superscripts denote ionized and neutral acceptors and donors; particle currents are:

(5) $j_n = -e[nv_n - D_n grad n], \qquad j_p = e[pv_p - D_p grad p]$

and diffusivities are governed by the Einstein relation. Avalanche generation [2] is:

(6) $G = a_n[\exp -(b_n/|F|)^m]|j_n|/e + a_p[\exp -(b_p/|F|)^m]|j_p|/e$

and the emissivity coefficients $e_1 ... e_4$ are:

(7) $e_1 = c_{nd} n_d + p c_{pd}$, $e_2 = c_{na} n_a + p c_{pa}$

$e_3 = c_{pa} p_a + n c_{na}$, $e_4 = c_{pd} p_d + n c_{nd}$

c_{nd}, c_{na}, etc., are capture coefficients [3]; n_d, p_d, etc., are obtained at equilibrium. The above equations are coupled through Poisson's equation, which in terms of energy is:

(8) $\nabla^2 E = -[c^2/\varepsilon][(n-p)-(N_d^+ - P_a^-)]$

The energy and potential are related, $E = -c\phi$; the field in equation (6) is $F = -\nabla\phi$.

THE RESULTS

All calculations were for the figure 1 shallow doping distribution, with the results dependent upon: (i) the Fermi level, (ii) the ratios P_a/N_d, and (iii) the trap density.

Low Bias Results: Resistivities and compensation estimates were obtained at low bias levels from the density distributions within the interior of the LT region. At a bias of 1.0 volts the results are similar to those at zero bias. As seen in table 1, the resistivities exceed 10^6 ohm-cm for donor traps at 10^{16}, and acceptor traps between 10^{17} and 10^{15}. The positions of the equilibrium Fermi level (above the valence band) for $N_d = 10^{18}$, and $N_a = (10^{16}, 10^{17}, 10^{18})$ are $E_f(ev) = (0.69, 0.63, 0.45)$, respectively. For $N_d = 10^{19}$, and $N_a = 10^{18}$, $E_f = 0.63$ev. The designation 'p' identifies the region as p-type, with the mobility dominated by holes. Table 2 displays the ionization of the traps at 1.0 v. The results indicate that within the insulating LT region $P_a^- \sim N_d^+$.

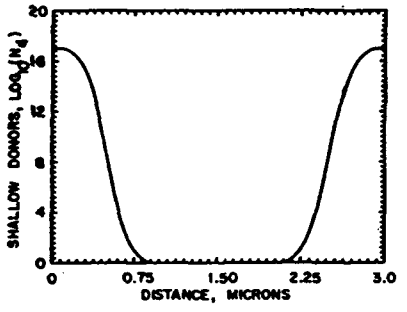

Figure 1. Shallow donor concentration of the N(LT)N structure.

$N_d(\downarrow)/P_a(\rightarrow)$	10^{18}	10^{17}	10^{16}	10^{15}
10^{19}	2.72x10^6 (p)	••	••	••
10^{18}	3.21x10^5 (p)	2.68x10^6 (p)	9.2410^6 (n,p)	4.75x10^7 (n)
10^{17}	5.49x10^1 (p)	3.18x10^3 (p)	2.45x10^6 (p)	••
10^{16}	7.16x10^0 (p)	••	••	••

Table 1. Resistivities (ohm-cm) of the LT region at 1.0 v.

$N_d(\downarrow)/P_a(\rightarrow)$	10^{16}	10^{17}	10^{18}	10^{19}
10^{19}	$P_a^- \sim P_a$, $N_d^+ \sim 0.1N_d$	••	••	••
10^{18}	$P_a^- \sim P_a$, $N_d^+ \sim N_d$	$P_a^- \sim P_a$, $N_d^+ \sim 0.1N_d$	$P_a^- \sim P_a$, $N_d^+ \sim 0.01N_d$	$P_a^- \sim P_a$, $N_d^+ < P_a$
10^{17}	$P_a^- \sim 0.1P_a$, $N_d^+ \sim N_d$	$P_a^- \sim P_a$, $N_d^+ \sim N_d$	$P_a^- \sim P_a$, $N_d^+ \sim 0.1N_d$	••
10^{16}	$P_a^- > N_d$, $N_d^+ \sim N_d$	••	••	••

Table 2. Approximate compensation conditions in LT region at 1.0 v.

Finite and High Bias, $N_d=0$: E_f is significantly below midgap. The results for:(i) P_a varying from 10^{16}/cm^3 to 10^{18}/cm^3, and (ii) $P_a > 10^{18}$/cm^3, are distinctly different. *For P_a varying from 10^{16}/cm^3 to 10^{18}/cm^3*, and at low voltage, charge neutrality within the LT region means $p \sim P_a^-$; and n is negligible. At elevated bias levels electrons are injected into the LT region and trapped by the acceptors. At sufficiently high bias, with the acceptor traps filled there is a significant increase in n, and a significant current increase. The electric field profile increases nearly linearly with distance. Further increases in bias result in avalanche multiplication. For larger P_a, higher bias is required to fill the acceptors, but the field profile within the structure is still linear. The relevant profiles for this calculation at a bias prior to breakdown are shown in figure 2, for $P_a = 10^{18}$/cm^3. *For $P_a > 10^{18}$/cm^3*, the kinetics is primarily that of holes within the valence band and the ionized deep acceptors, whose concentration is approximately two orders of magnitude below the total trap density. There is near charge neutrality within the LT region except at the downstream (LT)N interface where a high concentration of ionized acceptor traps forms, with a reduction of mobile holes. There is also a zone depleted of electrons within the heavily doped N region. One observes the formation of a pn junction region as a result of the trap dynamics, with the generation of a local high value of electric field. *As a result avalanching occurs at lower values of voltage, than for the lower P_a study.* The high P_a study is displayed in figure 3.

The situation for $N_d \neq 0$ is qualitatively different, although there are ostensible similarities. For example with $N_d = 10^{17}$/cm^3 and $P_a = 10^{18}$/cm^3 the field profile is qualitatively similar to figure 3. The difference is that the acceptor ionization is accompanied by ionized deep donors, as seen in figure 4. The breakdown characteristics are similar to the $N_d = 0$ study. The situation when $N_d = P_a = 10^{18}$/cm^3, displays characteristics that appear as a hybrid of the calculations of figures 2 and 3. At voltages up to and near 20 volts the field distribution is qualitatively similar to that of figure 3, although the peak field is approximately 60 kv/cm less. Further bias increases result in modest changes in the n and p profiles within the LT region, but an increasing share of the voltage drop across the LT region. Breakdown occurs at much higher voltage levels. *The current voltage characteristics for a select set of trap densities are displayed in figure 5. The trap density dependence of breakdown is shown in table 3.*

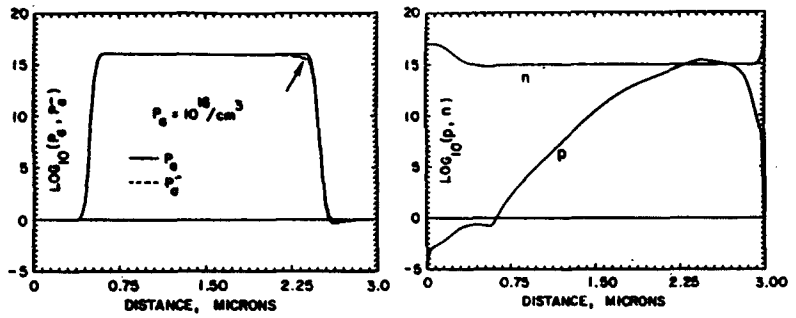

Figure 2. (a) Total and ionized trap distribution at a bias of 45 v. (2b). Distribution of electrons and holes.

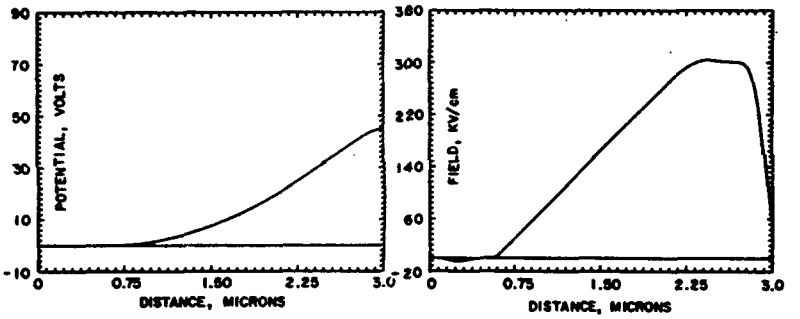

Figure 2c. Potential and electric field distribution at 45 v.

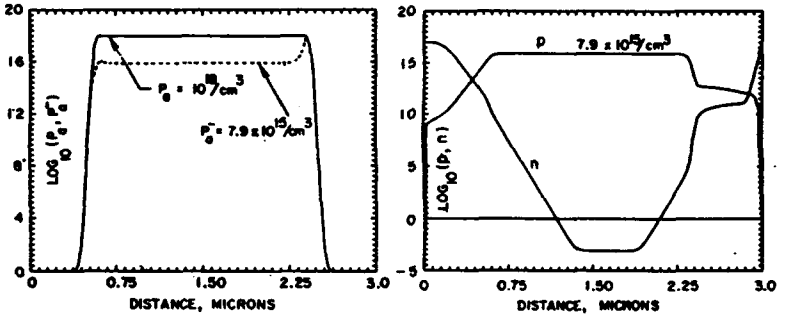

Figure 3. (a) Total and ionized trap distribution at 21v. (3b). Distribution of n and p.

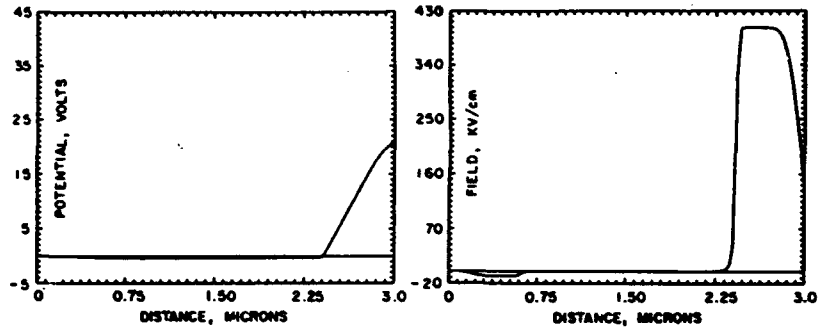

Figure 3c. Potential and electric field distribution at 21 v.

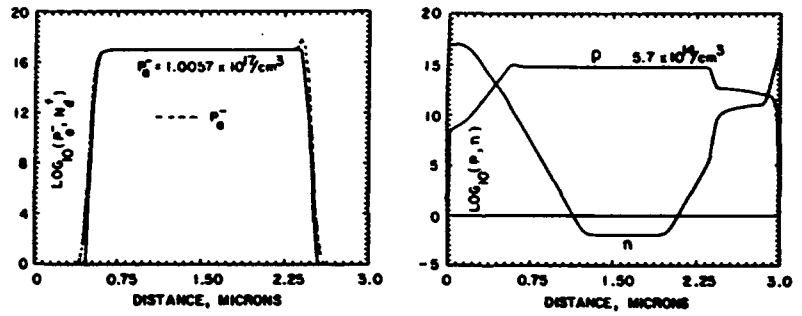

Figure 4. As in figure 3 but for $P_a = 10^{18}$, $N_d = 10^{17}$, at 20v.

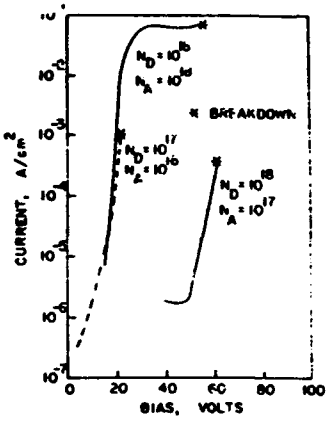

Figure 5. Current voltage characteristics to breakdown for different trap densities.

$N_d(\downarrow)/P_g(\rightarrow)$	10^{16}	10^{17}	10^{16}	10^{15}	10^{14}
0	21 v	25 v	45 v	40 v	28 v
10^{16}	21 v	••	47 v	••	••
10^{17}	21 v	45 v	••	••	••
10^{18}	55 v	62 v	48 v	40 v	30 v
10^{19}	70 v	••	••	••	••

Table 3. Breakdown voltages for different densities of traps.

SUMMARY

The conclusion of this study is that the electrical characteristics of N(LT)N structures are dependent in a very sensitive way on the distribution of traps. The calculations strongly suggest that for N(LT)N structures, the low voltage and high voltage electrical characteristics may provide a signature of the relative density of donor and acceptor traps. Of particular importance is the development of pn [4] junction behavior and low breakdown voltages for acceptor trap dominated material. It is anticipated that the details of the results will depend upon the doping levels of the shallow cladding regions; preliminary studies, however, do not reveal significant qualitative dependencies.

ACKNOWLEDGEMENT

This study was supported by AFOSR.

REFERENCES

1. F. W. Smith, MIT Doctoral Dissertation (1991)
2. M. Kurata, *Numerical Analysis for Semiconductor Devices*, D. C. Heath and Co. MA (1982)
3. K. Horio, T. Ikoma and H. Yanai, IEEE Trans. Electron Devices *ED-33*, 1985 (1986).
4. P. M. Solomon and K. Weiser, J. App. Phys. *70*, 5408 (1991).